

Hybrid Inverse Airfoil Design Method for Complex Three-Dimensional Lifting Surfaces

Ashok Gopalarathnam*

North Carolina State University, Raleigh, North Carolina 27695

and

Michael S. Selig†

University of Illinois at Urbana—Champaign, Urbana, Illinois 61801

A method is presented for inverse design of airfoils for complex three-dimensional wings in incompressible flow. The method allows for prescription of inviscid velocity distributions over different cross sections of the wing in a multipoint fashion. A hybrid approach is used to determine the shapes of the wing cross sections that satisfy the design specifications. The airfoils forming the cross sections of the wing are generated using an inverse code for isolated airfoil design. A three-dimensional panel method is then used to obtain the velocity distributions over the resulting wing. The isolated airfoil velocity distributions are then used as design variables in a multidimensional Newton iteration method to achieve the design specifications on the wing. The method is particularly useful for complex geometries such as junctures, where three-dimensional and interference effects have to be accounted for in the design process. A key feature of the design method is a scheme to avoid using the panel method for sensitivity computations for the Newton iterations. This scheme not only results in significant reductions in computation time but also enables the integration of any readily available three-dimensional analysis code in executable form. Examples are shown to demonstrate the usefulness of the method.

Nomenclature

C_l	=	airfoil lift coefficient, chord = 1
c	=	airfoil/section chord
F	=	vector containing the residuals
J	=	Jacobian matrix
n	=	number of design variables
V	=	airfoil/section velocity nondimensionalized by the freestream velocity
v	=	desired value for the velocity difference over a segment
α	=	angle of attack, deg
ΔV	=	velocity difference over a segment normalized by the freestream velocity
δx	=	vector containing the corrections to the design variables

Subscripts

i	=	index of design variable for the Newton iteration
r	=	property associated with the wing root
t	=	property associated with the wing tip
w	=	property associated with the wing
$2D$	=	property associated with an airfoil in isolation
$3D$	=	property associated with a cross section of a three-dimensional lifting surface

Introduction

A HYBRID method has been developed for wing design. The method uses an approach similar to the one developed by the

authors for inverse design of multielement airfoils¹ in potential flow, which was subsequently extended to handle viscous inverse design.² This multielement airfoil design method uses a novel hybrid approach by coupling an isolated airfoil design code^{3,4} (PROFOIL) with a two-dimensional panel method. The inverse airfoil design code is used to design the elements of the multielement airfoil in isolation, and the panel method is then used to analyze the resulting multielement airfoil. An integral boundary-layer method is then used to obtain the boundary-layer developments on the individual elements. By using a multidimensional Newton iteration procedure, the design variables associated with the isolated airfoil design are adjusted to achieve desired velocity and boundary-layer prescriptions on the elements of the multi-element airfoil. A key feature of the method is a scheme for rapid computation of the Newton iteration sensitivities without using the panel method. This scheme was developed based on the observation of similarities¹ in the changes in velocity distributions for an airfoil in isolation and as a part of the multielement airfoil. The hybrid approach as well as the sensitivity computation scheme enable rapid, interactive design even with several multipoint viscous prescriptions.²

Several experiences with successful applications of the isolated airfoil design method^{5,6} and the more recent hybrid approach for rapid, interactive multielement airfoil design⁷ have naturally prompted the question of whether such an approach can be used for designing complex three-dimensional wings. This paper presents the extension of the hybrid approach to three-dimensional aerodynamic systems. More specifically, the current work describes a potential-flow method for designing the shapes of wing cross sections to achieve multipoint prescriptions in velocity distributions. For this purpose the isolated airfoil design code^{3,4} (PROFOIL) is used to generate the airfoils that form the cross sections of the three-dimensional aerodynamic system, and a three-dimensional analysis method (the panel method PMARC/CMARC^{8,9} in this paper) is used to analyze the resulting wing system. The variables associated with the design of the airfoils in isolation are then adjusted to achieve the prescriptions on the wing cross sections. The paper shows that, as with the multielement airfoil design problem, there are similarities in the velocity-distribution changes for an airfoil in isolation and as part of a complex three-dimensional system. This similarity is used to an advantage to avoid repeated panel method analyses for the sensitivity computation via finite differencing. Instead, the

Presented as Paper 99-0401 at the AIAA 37th Aerospace Sciences Meeting and Exhibit, Reno, NV, 11–14 January 1999; received 29 March 1999; revision received 29 January 2002; accepted for publication 1 February 2002. Copyright © 2002 by Ashok Gopalarathnam and Michael S. Selig. Published by the American Institute of Aeronautics and Astronautics, Inc., with permission. Copies of this paper may be made for personal or internal use, on condition that the copier pay the \$10.00 per-copy fee to the Copyright Clearance Center, Inc., 222 Rosewood Drive, Danvers, MA 01923; include the code 0021-8669/02 \$10.00 in correspondence with the CCC.

*Assistant Professor, Department of Mechanical and Aerospace Engineering, Box 7910; ashok-g@ncsu.edu. Member AIAA.

†Associate Professor, Department of Aeronautical and Astronautical Engineering, 306 Talbot Laboratory, 104 S. Wright Street; m-selig@uiuc.edu. Senior Member AIAA.

sensitivities are computed directly during the isolated airfoil design, saving computational time. In addition, this sensitivity computation scheme enables easy integration of any three-dimensional analysis method in executable form in the current design code.

It is illustrative to compare the current approach to the design approaches used in existing three-dimensional inverse design methods. In a broad sense inverse design methods for wings can be classified into two categories: 1) methods for spanwise design,^{10–12} which are frequently used to minimize induced drag or specify spanwise properties such as circulation, lift coefficient, or downwash variations (The design variables for these methods are usually spanwise variations of chord, twist, or other such geometric properties.); and 2) methods for specifying desired chordwise velocity distributions at several sections along the wing.

In the current work the emphasis is on methods for chordwise inverse design to provide airfoil shapes that when used as cross sections for the three-dimensional wing will provide desired velocity distributions on the wing. It is intended that the current design method be used in conjunction with a method for spanwise inverse design. The spanwise variations of chord, twist, etc., are provided as inputs to the current method, and they remain unaltered during the inverse design.

The methods currently in existence for chordwise inverse design typically use the following steps in the design process:

- 1) Start with initial shapes for the airfoils.
- 2) Obtain the velocity distributions over the wing using an appropriate analysis method.
- 3) Compare the velocity distributions from step 2 with the target distributions prescribed by the designer.
- 4) Use the difference in the velocity distributions to predict the changes in airfoil shapes necessary to better match the prescribed velocity distributions.

The methods typically loop through steps 2–4 until convergence is achieved.

A relatively early example of a such a design method is that of Bristow and Hawk.^{13,14} In their method a panel method is first used to analyze the baseline configuration. To predict the effect of changes in geometry (step 4), a matrix containing the partial derivatives of the potential at each point with respect to each geometry parameter is used to compute the new potential and subsequently the new velocities. These derivatives of the potential are computed using a first-order expansion to the panel-method equations. A more recent design method has been published by Campbell and Smith¹⁵ in 1987 for transonic wings and later extended in 1992 to wing-body-nacelle configurations.¹⁶ In this method an algorithm that relates changes in local velocity to changes in surface curvature is used in step 4 to compute the changes in airfoil shapes required to better match the target velocity distribution. A transonic small-disturbance code that can handle complex three-dimensional geometries is used as the analysis module. Other examples are an inverse method for transonic wing design¹⁷ and the more recent method of Hassan and Charles¹⁸ for the design of airfoils for helicopter rotor blades.

The current method takes a slightly different approach. Instead of specifying velocity distributions for an entire wing cross section, the airfoils that form the cross section are divided into several segments. Over the segments selected by the designer, the desired velocity distribution for the wing along with the design condition (wing angle of attack) are prescribed. By using this approach, the difficulties that are sometimes associated with the specification of the velocity distribution for an entire cross section (such as the need to accurately guess the stagnation-point location) are avoided. In addition, multipoint specifications are possible. That is, certain segments of the wing can be designed for one angle of attack, while some other segments can be designed for a different angle of attack. Such a multipoint method avoids the tedium that is frequently associated with designing at a single condition and determining the off-design behavior via postdesign analysis.

The following sections provide a brief description of the current design method and the novel approach to sensitivity computation. It must be mentioned that the layout of the discussion in these two sections are similar to the corresponding sections in the papers on

the multielement airfoil design method.^{1,2} They have, however, been adapted and included here for completeness. Three example design problems are then presented to demonstrate the method.

Design Methodology

As mentioned earlier, the current three-dimensional inverse design method IWING uses a hybrid approach by coupling the isolated inverse airfoil code PROFOIL^{3,4} with a three-dimensional analysis method. In the current paper the panel code CMARC⁹ is used as the three-dimensional analysis method. The following subsections briefly describe the relevant features of PROFOIL and CMARC. A subsection on IWING then describes the coupling of the CMARC code with PROFOIL for inverse design of wing cross sections.

PROFOIL

PROFOIL is an inverse airfoil design method^{3,4} based on conformal mapping. In the method the airfoil is divided into several segments. The method allows specification of a velocity difference ΔV_{2D} (for the airfoil in isolation) over each segment along with a design C_l for that segment. Figure 1 shows the definition of ΔV as used in this paper. In addition, it is also possible to specify a nonlinear velocity distribution over the segment^{3,4} for the airfoil in isolation by defining a fixed number of nodes through which a spline is passed.

An important feature of the method is the multidimensional Newton iteration scheme. The scheme allows the designer to selectively give up control on some of the parameters used in conformal mapping and in the isolated airfoil design in order to achieve specified values for other design specifications. For example, it is possible to vary the values of the design angles of attack for all segments on the upper surface to achieve a desired maximum thickness, while varying the corresponding values for segments on the lower surface to achieve a desired value of the maximum camber. Thus, multipoint specification can be handled. Also the velocity difference ΔV over any segment or the velocity values at the nodes of a segment with a nonlinear velocity specification can be selected for iteration in the Newton method. The power and flexibility of this inverse design method has been used in several applications including the design of high-lift airfoils⁵ for low-Reynolds-numbers applications and the design of families of natural-laminar-flow airfoils⁶ for low-speed applications.

CMARC

CMARC⁹ is an enhanced, C-language version of the well-known three-dimensional panel-code PMARC⁸ version 12, which was developed at the NASA Ames Research Center. CMARC is a low-order panel code for solving flows around arbitrary three-dimensional configurations in inviscid, incompressible flows. The surface of the three-dimensional wing/body is divided into several panels. Constant-strength source and doublet distributions are assumed over each panel. Wakes are shed from the trailing edges of wings and are also discretized into panels that have constant-strength doublet distributions. The matrix solution is performed using a fast,

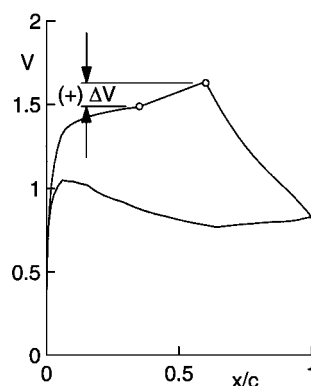


Fig. 1 Definition of ΔV for a segment as denoted by the segment endpoints.

iterative solver¹⁹ that does not require the whole influence coefficient matrix to be stored in memory.

Although CMARC has the capability for time stepping the wakes to simulate wake roll up, an initial, rigid wake was used for all of the examples in this paper, and no time stepping was done to keep the time for each analysis as short as possible.

IWING

The following sequence of steps provide an overview of the approach used in the current design method in coupling PROFOIL and CMARC for achieving desired velocity distributions on wing cross sections.

1) Generate the individual airfoils for the wing cross sections using PROFOIL.

2) Scale and position the resulting airfoils according to the specified wing geometry.

3) Analyze the wing using CMARC, and obtain the inviscid velocity distributions over the cross sections at the various operating points. The section velocity distributions are obtained by neglecting the spanwise components of the surface velocity normal to the section.

4) Compare the inviscid velocity difference ΔV_{3D} over the design segments on the wing with the correspondingspecifications. It is unlikely, however, that these ΔV_{3D} values will match the specifications.

5) Adjust the isolated airfoil velocity difference ΔV_{2D} for each design segment using a Newton iteration scheme to achieve desired values of the wing ΔV_{3D} over the corresponding segments.

It must be mentioned that the isolated airfoil C_l at which the velocity difference ΔV_{2D} is evaluated in step 5 is determined by the requirement that the stagnation points on the isolated airfoil and on the corresponding section of the wing occur at the same geometric location for the wing operating point under consideration. As detailed in Ref. 20, this requirement is necessary, particularly when considering segments close to the leading edges of the sections.

The design methodology for the inverse wing design approach is first illustrated using a low-aspect-ratio planar wing as an example. It is emphasized that this wing and other wings in this paper merely serve as examples and are not intended for any application. Figure 2 shows the planform of the low aspect ratio wing used for the first example. This wing has an aspect ratio of 2.67 and has zero dihedral. Two operating conditions are considered. The first corresponds to a wing angle of attack of 3.6 deg, and the second corresponds to an angle of attack of 9.4 deg. For this example two cases are considered. The first focuses on the segment r on the upper surface of the root section at the first operating condition, and the second case focuses on the segment t on the lower surface of a section at 95% semispan (close to the tip) at the second operating condition. In each case the isolated airfoil velocity difference ΔV_{2D} over the segment is varied to study its effect on the velocity distributions over the two wing cross sections under consideration, in particular the ΔV_{3D} over the corresponding segments.

Figures 3a–3e show the results of varying ΔV_{2D} for the segment r on the upper surface of the wing root. Figure 3a shows the three geometries and velocity distributions for the root airfoil in isolation with $\Delta V_{2D,r} = -0.1, 0$, and $+0.1$ and $C_l = 0.9$. Figure 3b shows the geometry and velocity distribution for the tip airfoil in isolation.

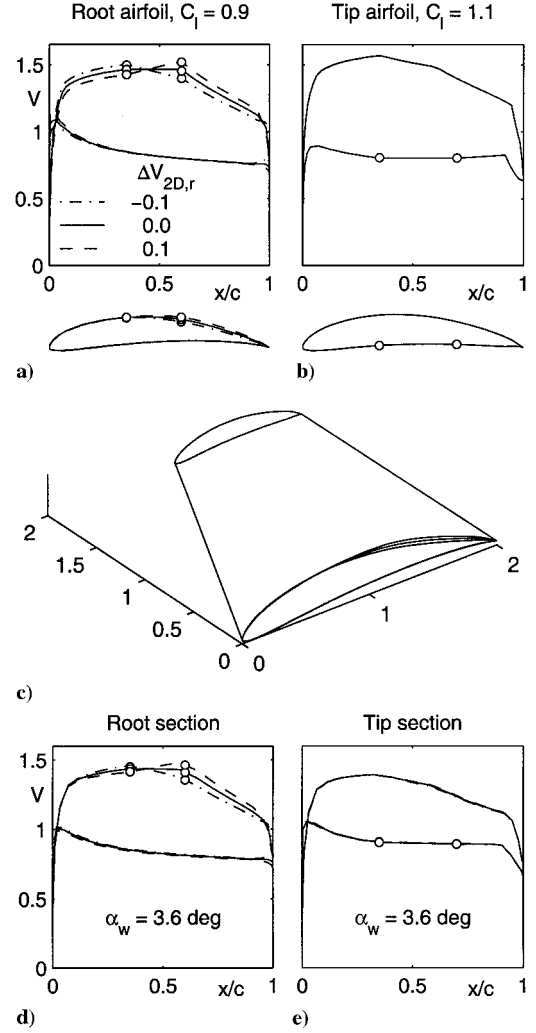


Fig. 3 Case 1: Velocity distributions over the a) root airfoils and b) tip airfoil in isolation, c) wing geometries, and velocity distributions over the wing d) root sections and e) tip sections at the first operating condition.

Figure 3c shows the three resulting wings. As seen in the figure, the tip airfoil is left unchanged for this case. Figures 3d and 3e show the three corresponding velocity distributions for the root and the tip sections of the wings at the first operating condition. The similarity in trends in the velocity distributions for the three isolated root airfoils and the corresponding root sections illustrates that the isolated airfoil velocity distribution is an effective design variable for the velocity distribution over the corresponding section on the wing. In spite of the low aspect ratio of the example wing, it is seen that changing the ΔV_{2D} for a segment results in a change in the ΔV_{3D} for the corresponding segment on the wing, with little change in the velocity distribution over other portions of the wing that have a different airfoil.

Figures 4a–4e show the results of varying $\Delta V_{2D,t}$ for the segment on the lower surface of the tip airfoil, with the root airfoil left unchanged. In this case the velocity distributions for the root and tip sections (Figs. 4d and 4e) correspond to the second operating condition. Again, the similarity in trends between the velocity distributions on the three isolated tip airfoils and on the corresponding tip sections is clearly seen.

Figures 5a and 5b show the changes in $\Delta V_{3D,r}$ and $\Delta V_{3D,t}$ resulting from perturbations to $\Delta V_{2D,r}$, with $\Delta V_{2D,t}$ kept unchanged at 0. Similarly, Figs. 5c and 5d show the changes in $\Delta V_{3D,r}$ and $\Delta V_{3D,t}$ resulting from perturbations to $\Delta V_{2D,t}$, with $\Delta V_{2D,r}$ kept unchanged at 0. Inspection of Figs. 5a–5d yields the following observations. First, perturbations to ΔV_{2D} for a particular segment result in an almost equal change in ΔV_{3D} for the same segment, that is,

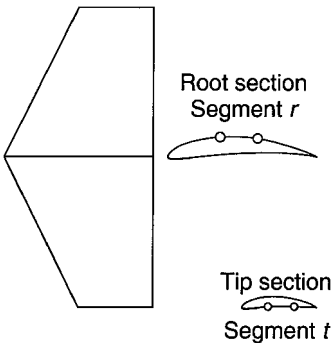


Fig. 2 Planform of the baseline low-aspect-ratio planar wing used to illustrate sensitivities.

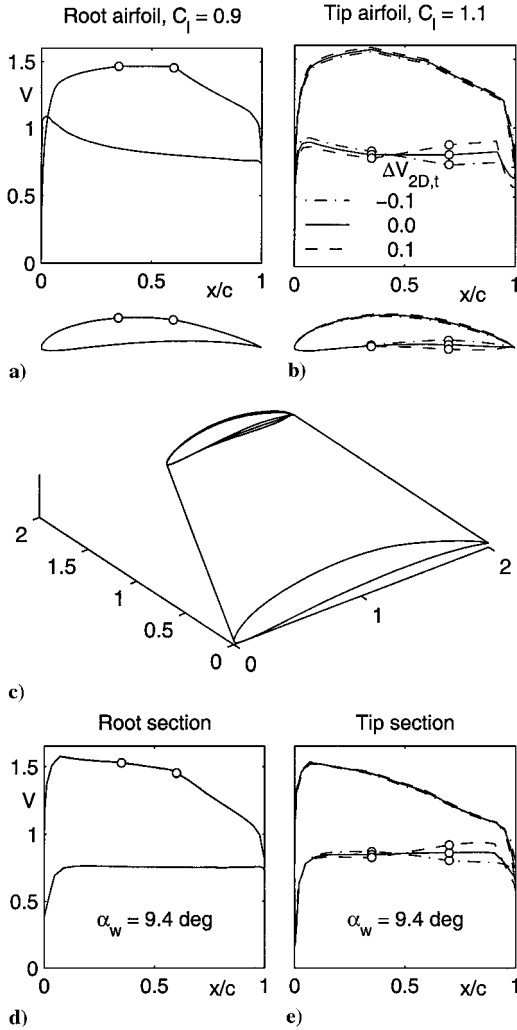


Fig. 4 Case 2: Velocity distributions over the a) root airfoil and b) tip airfoils in isolation, c) wing geometries, and velocity distributions over the wing d) root sections and e) tip sections at the second operating condition.

$$\frac{\partial \Delta V_{3D,r}}{\partial \Delta V_{2D,r}} = \mathcal{O}(1) \quad (1)$$

$$\frac{\partial \Delta V_{3D,t}}{\partial \Delta V_{2D,t}} = \mathcal{O}(1) \quad (2)$$

where $\mathcal{O}(1)$ denotes “of the order of 1.” Second, the cross-coupling effects, such as the change in ΔV_{3D} for a segment on one section resulting from a perturbation to ΔV_{2D} for a segment on another airfoil, are comparatively small, that is,

$$\frac{\partial \Delta V_{3D,r}}{\partial \Delta V_{2D,t}} \ll \frac{\partial \Delta V_{3D,r}}{\partial \Delta V_{2D,r}} \quad (3)$$

$$\frac{\partial \Delta V_{3D,t}}{\partial \Delta V_{2D,r}} \ll \frac{\partial \Delta V_{3D,t}}{\partial \Delta V_{2D,t}} \quad (4)$$

These two cases show that even for a low-aspect-ratio wing the isolated airfoil velocity difference ΔV_{2D} for a segment is an effective design variable for the ΔV_{3D} for the corresponding sections on the wing.

The second example presents the similarity in trends in the velocity distributions for a complex nonplanar wing. For this example the nonplanar wing shown in Fig. 6 is used. In this example the ΔV_{2D} on a segment on the upper surface of the wing airfoil (airfoil B in the figure) at the wing-winglet juncture is varied to study its effect on

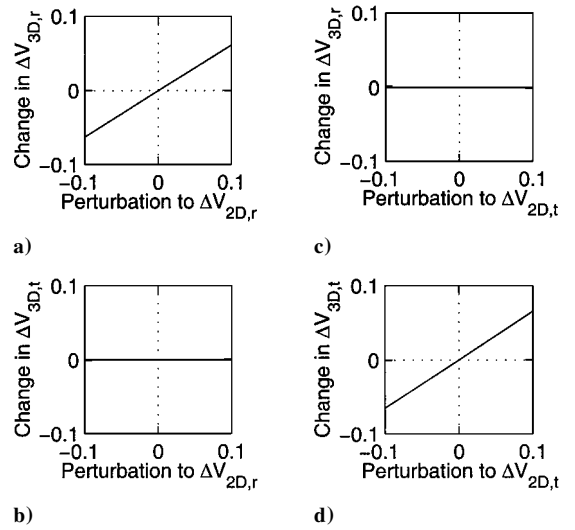


Fig. 5 Changes in $\Delta V_{3D,r}$ and $\Delta V_{3D,t}$ resulting from perturbations to $\Delta V_{2D,r}$ and $\Delta V_{2D,t}$.

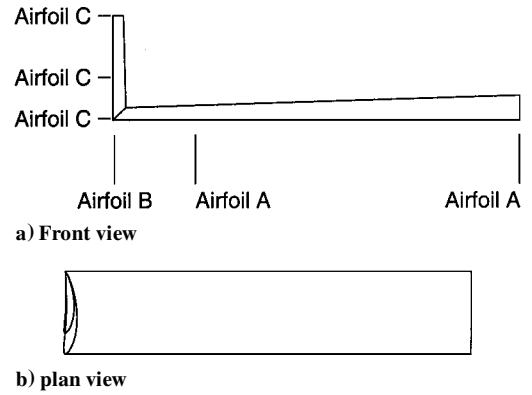


Fig. 6 Nonplanar wing used to illustrate sensitivities.

the velocity distribution at a section close to the juncture at an angle of attack α_w of 10 deg. As shown in the figure, the juncture section is formed by finding the contour resulting from the intersection of the tip section of the wing and the root section of the winglet. Because of the juncture geometry, the velocity distribution close to the juncture is significantly different from the velocity distribution over the regions of the wing away from the juncture. This example, therefore, demonstrates the need for an inverse method that can take into consideration the complex three-dimensional effects of such junctures while designing the shape of the juncture airfoils.

Figure 7a shows the isolated airfoil velocity distributions for airfoil B with three values of ΔV_{2D} for the segment on the upper surface. The corresponding three velocity distributions for the section at the wing-winglet juncture are shown in Fig. 7b. A comparison of the three velocity distributions for the airfoils in isolation and for the sections at the juncture shows that the similarity in changes in the velocity distributions observed earlier for the planar wing example is also observed for this example with the more complex juncture section. Figure 8 shows the changes in the ΔV_{3D} for perturbations to ΔV_{2D} for the segment under consideration. As seen from the figure, even for a segment close to a juncture, changes in ΔV_{2D} result in a linear and an almost equal change in ΔV_{3D} . This example clearly demonstrates the foundations upon which the new design method depends.

Thus, by using a multidimensional Newton iteration it is clearly possible to control the ΔV_{3D} for several segments on the cross sections of a wing (each at a different operating point) simultaneously using the values of ΔV_{2D} for the corresponding segments as design variables. Moreover, the direct and near linear connection between

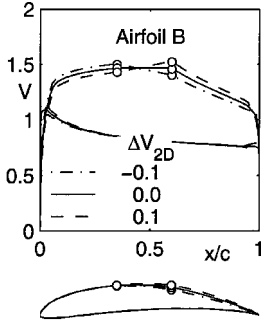


Fig. 7a Geometries and velocity distributions for the airfoil B.

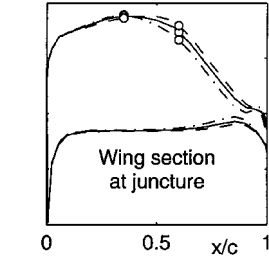


Fig. 7b Velocity distributions at the wing section close to the juncture.

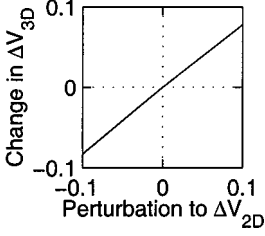


Fig. 8 Changes in ΔV_{3D} resulting from perturbations to ΔV_{2D} for the segment at the section close to the juncture.

ΔV_{2D} and ΔV_{3D} is true even for regions where the three-dimensional effects are high, such as on low-aspect-ratio wings and in complex juncture regions as shown by the two examples.

Sensitivity Computation

Typically, a system of n nonlinear equations can be solved by an n -dimensional Newton iteration, where a matrix equation is solved during each step of the iteration. This matrix equation can be written as²¹

$$\mathbf{J} \cdot \delta \mathbf{x} = -\mathbf{F} \quad (5)$$

where \mathbf{F} is an n -dimensional vector containing the residuals of the functions f_i to be zeroed, $\delta \mathbf{x}$ is the n -dimensional vector containing the corrections required to the n design variables x_i to bring the vector \mathbf{F} closer to zero, and \mathbf{J} is the $n \times n$ Jacobian of the system containing the gradient information. For each step of the iteration, \mathbf{F} and \mathbf{J} are determined, and $\delta \mathbf{x}$ is computed using Eq. (5). The corrections are then applied to the design variables to bring the residuals closer to zero.

The most obvious scheme to compute the Jacobian \mathbf{J} would have been to use finite differencing to evaluate the gradients numerically using the panel method. In this scheme, for an n -dimensional Newton iteration the panel-method analysis would have to be performed n times to determine the Jacobian just for a single step in the iteration. The major shortcoming of this approach is that calculating the Jacobian by repeated panel-method analyses is computationally expensive, with the cost increasing with increasing number of design variables and number of panels used for the panel-method analysis. For instance, in the multielement airfoil design method¹ it was demonstrated that for a design example with several multipoint design prescriptions the CPU time was reduced by a factor of 32 from 16,586 s (4.6 h) to just 520 s (8.7 min) by an alternate scheme that avoided using the panel method for computing the sensitivities.

This cost of repeated panel-method analyses for sensitivity calculations can perhaps be significantly reduced by not recomputing the influence coefficient matrix (which determines the influence caused by the doublet/source strength on a panel on the flow conditions at another panel) during the gradient evaluations. However, with several legacy three-dimensional panel codes this approach may not be possible. In any case a method that can bypass having to perform several panel-method evaluations is likely to be computationally less expensive than the approach already described. It is therefore worthwhile searching for an alternative scheme to compute the Jacobian without using the panel method.

As done in the multielement airfoil design method,¹ the high cost associated with obtaining gradient information through the panel method can be bypassed by instead obtaining the approximate gradient information using the isolated airfoil velocity difference over the segments being considered. In other words, if y_r is any design variable associated with the design of the root airfoil, the gradient is

$$\frac{\partial \Delta V_{3D,r}}{\partial y_r} = \frac{\partial \Delta V_{3D,r}}{\partial \Delta V_{2D,r}} \frac{\partial \Delta V_{2D,r}}{\partial y_r} \quad (6)$$

Based on the results shown in Figs. 5a–5d, if we take $\partial \Delta V_{3D,r} / \partial \Delta V_{2D,r} \approx 1$ then Eq. (6) becomes

$$\frac{\partial \Delta V_{3D,r}}{\partial y_r} \approx \frac{\partial \Delta V_{2D,r}}{\partial y_r} \quad (7)$$

and similarly

$$\frac{\partial \Delta V_{3D,i}}{\partial y_i} \approx \frac{\partial \Delta V_{2D,i}}{\partial y_i} \quad (8)$$

These approximations to the gradients $\partial \Delta V_{2D,r} / \partial y_r$ and $\partial \Delta V_{2D,i} / \partial y_i$ can now be computed directly during the design of the isolated airfoil for the wing section under consideration, making it unnecessary to use the panel method for gradient calculations. Instead the gradient information is determined through the rapid conformal mapping method used to generate the isolated airfoils. The significance of the time savings resulting from this alternate approach to sensitivity computation can be understood by noting that a single CMARC analysis can take anywhere from ≈ 10 s of run time on a modern workstation for a simple geometry to a few minutes for more complex geometries. In contrast, a single conformal mapping calculation in PROFOIL takes just ≈ 0.04 s of run time and is independent of the complexity of the paneled geometry. As shown in Ref. 22 for two-dimensional design problems, the present method for computing the sensitivities is faster than computing the sensitivities from a first-order expansion of the panel method as was done by Bristow and Hawk.^{13,14} This faster sensitivity computation with the present method is primarily because there is no need for additional computation of the matrices containing the first-order expansion information with every full-panel-method computation.

Of course, by not using the panel method for computing the Jacobian the terms coupling the root and tip sections remain uncomputed. In other words, for a design variable associated with the root section y_r the gradient $\partial \Delta V_{3D,i} / \partial y_r$ can be computed only by using the panel method. This gradient can be expressed as

$$\frac{\partial \Delta V_{3D,i}}{\partial y_r} = \frac{\partial \Delta V_{3D,i}}{\partial \Delta V_{2D,r}} \frac{\partial \Delta V_{2D,r}}{\partial y_r} \quad (9)$$

Using Eqs. (3) and (4), however, we can make the approximation that $\partial \Delta V_{3D,i} / \partial y_r \approx 0$ and likewise $\partial \Delta V_{3D,r} / \partial y_i \approx 0$. Thus, in the present method the Jacobian is computed directly during the design of the isolated airfoils for the wing sections. The panel-method evaluation is necessary only for computing the residuals \mathbf{F} , reducing the number of panel-method analyses from $n + 1$ to 1 for each step of the Newton iteration. This reduction in the number of panel-method evaluations results in significant savings in computational time. It is emphasized that although the approximate gradients are computed without using the panel method the residuals for every step of the Newton iteration are still computed using the full panel method. It is for this reason that the current design method will work even for cases when there is a strong cross-coupling effect between design segments on different sections. Such strong cross-coupling effects can occur on low-aspect-ratio wings and design sections that are in the vicinity of wing-wing junctures.

In addition, by not relying on repeated panel-method runs to compute sensitivities to small changes in design variables (and hence, small changes in the resulting airfoil shapes) it is not necessary to pass information between PROFOIL and the panel method with a very high precision. As a result, the panel method does not have to be

integrated with PROFOIL in subroutine form, but instead can be executed using a system call. Information to and from the panel method can then be passed by programming PROFOIL to write the input files needed by the panel method, then execute the panel method using a system command, and finally read the output of the panel method to compute the ΔV_{3D} for the different design segments. This simplification in program integration has the important advantage that an executable for a different three-dimensional analysis method such as VSAERO can be easily substituted for the CMARC executable used in the current implementation. The only effort required for such a substitution is that a routine for writing the input file and another for reading the output of the new analysis method need to be coded. It is well known that modern three-dimensional aerodynamic analysis codes are quite complex and have been developed and refined after several thousand man hours of effort. Thus, by being able to “plug in” a ready-to-run executable for such an analysis code the significant time and effort that would have otherwise been spent in recoding and integrating the analysis code as a subroutine are saved.

Demonstration

The current design approach is demonstrated using three examples. It is emphasized that none of these examples are intended for any aircraft application; they were generated solely for the purpose of demonstrating the method. The first example considers a nonplanar wing at one wing angle of attack α_w and demonstrates how the current method can be used to achieve a desired velocity distribution over a segment in a complex juncture region. The second example demonstrates the capability to achieve desired velocity distributions on a section of a highly swept wing at two different wing angles of attack α_w . The third example further illustrates the multipoint capability by using a joined-wing configuration and considering two different segments each on a different wing and at a different α_w .

Figure 9 shows the geometry of the nonplanar wing used in the first example. Also seen is the distribution of the panels used for this demonstration. It must be mentioned that the “dished” appearance of the wing geometry near the juncture is a visual illusion resulting from the variation in the spanwise coordinates of the panel corner points. As seen in Fig. 10, airfoil A is used on the wing from the root to the 80%-semispan location. From this location the airfoils blend to airfoil B at the wing-winglet juncture. Airfoil C is used over the entire winglet. The juncture is formed by finding the contour of intersection of the wing tip and the winglet root sections.

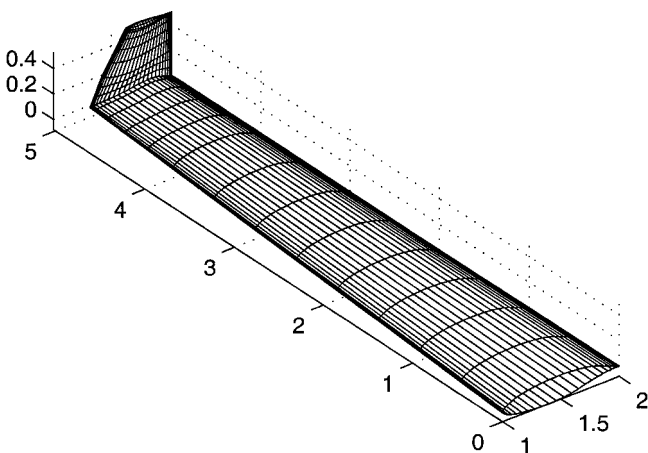


Fig. 9 Geometry of the nonplanar wing used for the first example.



Fig. 10 Front view of the geometry with airfoils labeled.

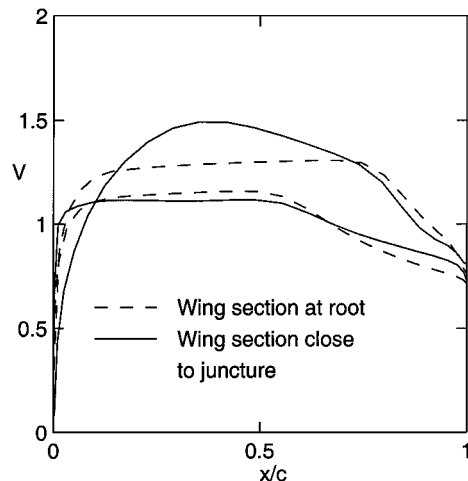


Fig. 11 Velocity distributions for two wing cross sections.

For the wing geometry used as the starting point for inverse design, airfoil B is taken to be identical to airfoil A. The wing is analyzed at an α_w of 0 deg. Figure 11 shows the inviscid velocity distributions for the wing sections at the root and at the juncture. In examining the upper-surface velocity distribution for the root section, it is seen that favorable velocity gradients exist to almost $0.7c$. As expected, this velocity distribution for the root section is nearly identical to the velocity distribution for the airfoil A in isolation (not shown in the figure) at the section C_l . Although the same airfoil is used at the juncture, the upper-surface velocity distribution is significantly different from that for the root section. This difference is a result of the effect of the winglet as well as the juncture. A constant velocity (zero gradient) is now prescribed for an upper-surface segment extending from $0.1c$ to $0.7c$ for the juncture section. The velocity distribution on the corresponding segment of airfoil B is varied to achieve this prescription. More specifically, the design variables used for iteration are the spline supports that define the two-dimensional velocity distribution over the corresponding segment on airfoil B.

Figure 12a compares the converged velocity distribution for the wing section at the juncture with the prescription for the section along with the initial velocity distribution for the section. It can be seen that the method has successfully satisfied the desired velocity prescription over the segment except for small deviations at the beginning and the end of the segment. These deviations are a result of the panel endpoints not coinciding with the endpoints of the segments. By increasing the number of chordwise panels, these deviations can be reduced. The significant change in the geometry of airfoil B as a result of satisfying the velocity prescription can be seen in Fig. 12b. This solution took approximately 147 s of run time on a 666 MHz Pentium III computer. Of this time 145 s were spent in the seven CMARC runs required for the Newton iteration to converge.

For the second example a 45-deg swept-back wing of aspect ratio 3 is considered. Figure 13 shows the wing planform. The geometry for this wing is generated such that the airfoils are parallel to the root and tip sections. As shown in Fig. 13, the design section near the middle of the wing half-span is perpendicular to the trailing-edge generator line of the wing. This design section is used for prescription of the surface velocity distributions on the wing. For the surface velocity distribution only the component of the surface velocity along the section is considered; the “spanwise” component of the surface velocity perpendicular to the section is ignored. This approach has also been used in Ref. 23 and results in a velocity distribution that has a stagnation point; the location of this stagnation point corresponds to the location of the attachment line on the swept wing.

Two segments are considered on the upper surface of the design section. The leading-edge segment is located between the section leading edge and $0.1c$. For this segment constant velocity is prescribed at α_w of 12 deg. The midchord section is located between

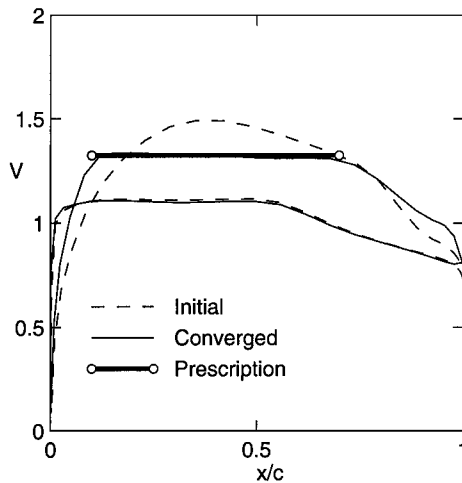


Fig. 12a Velocity distributions for the wing cross section close to the juncture for the initial and converged cases compared with the prescription.

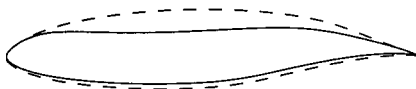


Fig. 12b Initial and final shapes for airfoil B.

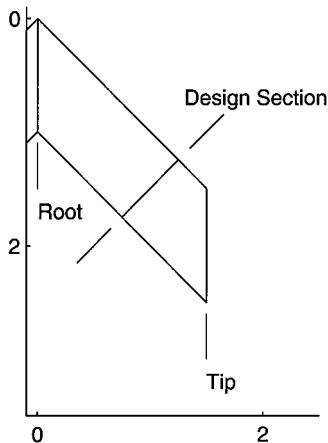


Fig. 13 Planform of the swept wing.

0.1c and 0.7c. For this segment the design prescription calls for constant velocity at α_w of 5 deg. Figure 14a shows the initial and converged velocity distributions for the design sections at the two angles of attack, along with the two design prescriptions. The initial and final airfoil geometries are shown in Fig. 14b. It can be seen that the method successfully achieves the prescriptions in the velocity, demonstrating that the hybrid approach is applicable not only for highly swept wings, but also for design segments that are located close to the leading edge.

For the third example the joined-wing configuration shown in Fig. 15 is used. It must be mentioned that the front and the rear wings are not joined in the model used in this study. By making this simplification in the model, the difficulty associated with paneling the joint is avoided. Because the objective of this work is to demonstrate the design approach, modeling the joint is not essential for the demonstration. Figure 16 shows the planview of the wing with the airfoils labeled. Two velocity prescriptions are made on two different segments: 1) a linear drop in velocity by 0.2 is prescribed for the lower-surface segment extending from 0.1c to 0.5c of the rear-wing section at the tip, and 2) constant velocity is prescribed on the upper-surface segment extending from 0.1c to 0.7c of the front-wing section at the tip. The design condition for the first prescription is an α_w of 0 deg, and the design variables for the Newton

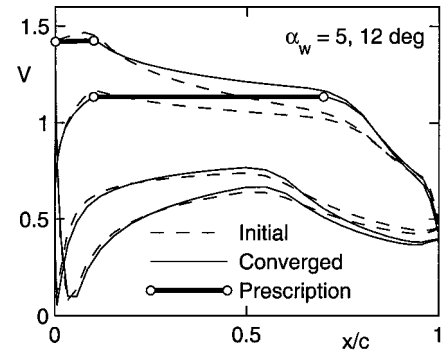


Fig. 14a Initial and converged velocity distributions for the design section along with the prescriptions.



Fig. 14b Initial and converged geometries for the airfoil.

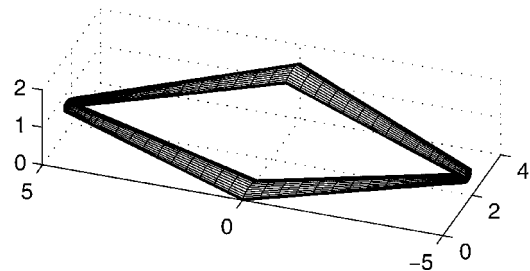


Fig. 15 Geometry of the joined wing used for the second example.

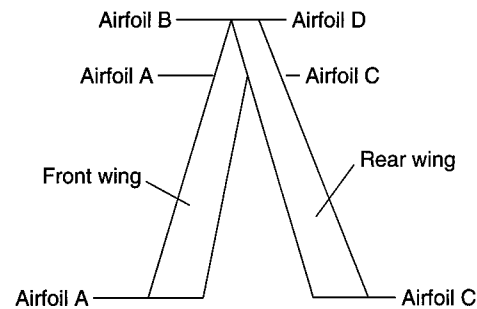


Fig. 16 Planview of the wing geometry with the airfoils labeled.

iteration are the spline supports that define the isolated-airfoil velocity distribution over the corresponding segment of airfoil D. For the second condition the design condition is an α_w of 5 deg with the design variables being the spline supports for the corresponding segment of airfoil B. It is emphasized that these prescriptions are to be satisfied simultaneously.

In solving design problems with multipoint prescriptions such as in the current example, it is often beneficial to perform the Newton iteration in stages. In the current example, for instance, the front-wing section is left unaltered in the first stage, and the rear-wing section is designed to satisfy the velocity prescriptions. With this new shape for the rear-wing section, the Newton iterations for the front-wing section are performed in the second stage. In the final stage the entire multipoint problem is solved by designing for the final shapes for both the sections simultaneously. All of these stages in the iteration are performed automatically in IWING.

Figure 17a compares the initial and converged velocity distributions for the segment on the rear-wing tip with the prescription for an α_w of 0 deg. It is seen that the method has been successful in satisfying the prescription even though the converged velocity

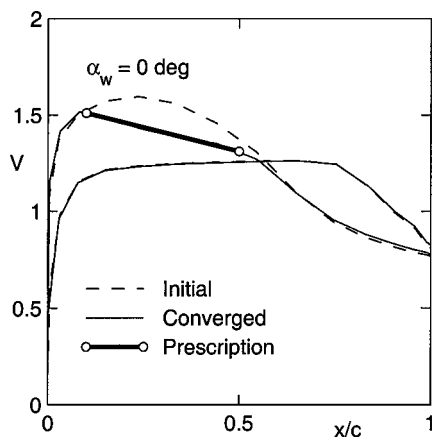


Fig. 17a Velocity distributions for the rear-wing cross section at the tip for the initial and converged cases compared with the prescription.



Fig. 17b Initial and final shapes for airfoil D.

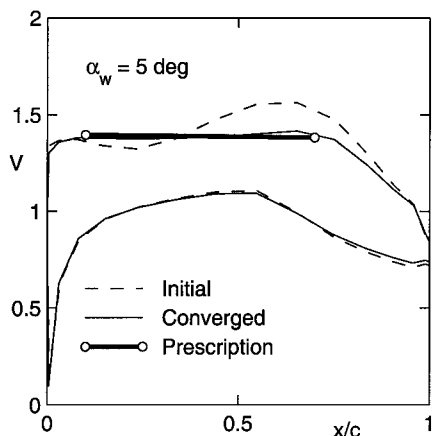


Fig. 18a Velocity distributions for the front-wing cross section at the tip for the initial and converged cases compared with the prescription.

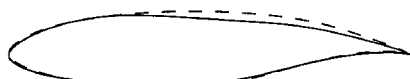


Fig. 18b Initial and final shapes for airfoil B.

distribution is significantly different from the initial distribution. Figure 17b shows the change in the shape of airfoil D as a result of satisfying the design prescription. The comparison of the initial and converged velocities for the segment on the upper surface of the front-wing tip with the design prescription at an α_w of 5 deg is shown in Fig. 18a. Again it is seen that the method has been successful in satisfying the prescription. The change in the geometry for this case is shown in Fig. 18b. This solution took about 91 s of run time on a 666 MHz Pentium III computer, of which about 89 s were spent on the 14 CMARC runs necessary for convergence. A total of 156 PROFOIL runs were made to compute the approximate sensitivities for this example. Had CMARC runs been used for this task instead of PROFOIL, it is likely that the run time for this example would have been increased by about 990 s or by about 11 times. This comparison illustrates the savings in time resulting from the approximate sensitivity computation scheme used in the current design method.

Conclusions

A hybrid approach that has proven successful in multielement inverse airfoil design has been extended to the inverse design of complex three-dimensional aerodynamic systems. More specifically, the design method described in the paper allows the design of airfoils for wing cross sections that achieve desired velocity distributions over specified segments at the corresponding design wing angles of attack. The airfoils for the wing cross sections are designed in isolation using an isolated-airfoil inverse method. The wing is then analyzed at the specified angles of attack using a three-dimensional panel method. The variables associated with the design of the airfoils in isolation are adjusted using a multidimensional Newton iteration scheme to achieve the specified velocity distributions on the wing. The formulation allows for design specifications on several segments of the wing, each at a different wing angle of attack, to be achieved simultaneously.

The paper shows that, as might be expected, there are similarities in changes in the velocity distributions for an airfoil in isolation and for the same airfoil when used as a part of a more complex aerodynamic system. Earlier work established this similarity for two-dimensional multielement airfoils. The current work demonstrates that the similarity is present even for three-dimensional systems. The current design approach makes use of this similarity in computing the sensitivities rapidly using the isolated airfoil design method rather than through repeated panel-method computations. In contrast with earlier wing inverse design approaches, there is no need for the computation of a first-order expansion to the panel-method equations. In addition, as the paper describes, this sensitivity computation scheme allows for easy integration of any analysis code in executable form for use in the current hybrid design approach.

Three examples are presented to demonstrate the design method. As shown in the paper, the method can handle design specifications on highly swept wings and even in complex juncture regions, where the velocity distributions for a section can be significantly different from those for the corresponding airfoil in isolation. In other words, the method is capable of designing wing sections in regions where there are strong three-dimensional effects. This capability in combination with the multipoint design capability makes the method a valuable tool for an airfoil/wing designer. The present potential flow design method can be particularly useful for rapid, interactive design of candidate wing shapes prior to postdesign analyses using computationally intensive viscous codes.

Acknowledgments

The authors wish to gratefully acknowledge the Boeing Company and technical monitors Steve D'Urso, Patrick Cassidy, Shawn Hagmeier, and Kentaro Sugiyama for supporting the initial phase of this work and the Ford Motor Company and technical monitors Frederico Hsu, Paul Carrannanto, and Paul Stanecki for supporting the second phase of this work.

References

- Gopalarathnam, A., and Selig, M. S., "Multipoint Inverse Method for Multielement Airfoil Design," *Journal of Aircraft*, Vol. 35, No. 3, 1998, pp. 398–404.
- Gopalarathnam, A., and Selig, M. S., "A Multipoint Viscous Design Method for Multi-Element Airfoils," AIAA Paper 98-2404, June 1998.
- Selig, M. S., and Maughmer, M. D., "A Multi-Point Inverse Airfoil Design Method Based on Conformal Mapping," *AIAA Journal*, Vol. 30, No. 5, 1992, pp. 1162–1170.
- Selig, M. S., and Maughmer, M. D., "Generalized Multipoint Inverse Airfoil Design," *AIAA Journal*, Vol. 30, No. 11, 1992, pp. 2618–2625.
- Guglielmo, J. J., and Selig, M. S., "High-Lift Low Reynolds Number Airfoil Design," *Journal of Aircraft*, Vol. 34, No. 1, 1997, pp. 72–79.
- Gopalarathnam, A., and Selig, M. S., "Low Speed NLF Airfoils: Case Study in Inverse Airfoil Design," *Journal of Aircraft*, Vol. 38, No. 1, 2001, pp. 57–63.
- Gopalarathnam, A., Selig, M. S., and Hsu, F., "Design of High-Lift Airfoils for Low Aspect Ratio Wings with Endplates," AIAA Paper 97-2232, June 1997.
- Ashby, D. L., Dudley, M. R., and Iguchi, S. K., "Development and Validation of an Advanced Low-Order Panel Method," NASA TM 101024, Oct. 1988.

- ⁹Pinella, D. F., and Garrison, P., "CMARC—A Three-Dimensional Panel Code," Aero-Logic, Los Angeles, CA, 1996.
- ¹⁰Jones, R. T., and Lasinski, T. A., "Effect of Winglets on the Induced Drag of Ideal Wing Shapes," NASA TM 81230, Sept. 1980.
- ¹¹Kroo, I. M., "A General Approach to Multiple Lifting Surface Design and Analysis," AIAA Paper 84-2507, Oct. 1984.
- ¹²Gopalarathnam, A., "Analysis of Ideal Non-Planar Wings," M.S. Thesis, Indian Inst. of Technology, Dept. of Aerospace Engineering, Madras, India, Oct. 1992.
- ¹³Bristow, D. R., and Hawk, J. D., "Subsonic Panel Method for the Efficient Analysis of Multiple Geometry Perturbations," NASA CR 3528, March 1982.
- ¹⁴Bristow, D. R., and Hawk, J. D., "Subsonic Panel Method for Designing Wing Surfaces from Pressure Distribution," NASA CR 3713, July 1983.
- ¹⁵Campbell, R. L., and Smith, L. A., "A Hybrid Algorithm for Transonic Airfoil and Wing Design," AIAA Paper 87-2552, Aug. 1987.
- ¹⁶Campbell, R. L., and Smith, L. A., "Application of a Direct/Iterative Design Method to Complex Transonic Configurations," NASA TP 3234, Oct. 1992.
- ¹⁷Silva, D. H., and Sankar, L. N., "An Inverse Method for the Design of Transonic Wings," AIAA Paper 92-1025, Feb. 1992.
- ¹⁸Hassan, A. A., and Charles, B. D., "Airfoil Design for Helicopter Rotor Blades—A Three-Dimensional Approach," *Journal of Aircraft*, Vol. 34, No. 2, 1997, pp. 197–205.
- ¹⁹Davidson, E. R., "The Iterative Calculation of a Few of the Lowest Eigenvalues and Corresponding Eigenvectors of Large Real-Symmetric Matrices," *Journal of Computational Physics*, Vol. 17, No. 1, 1975, pp. 87–94.
- ²⁰Gopalarathnam, A., "Hybrid Methods for Inverse Aerodynamic Design," Ph.D. Dissertation, Univ. of Illinois at Urbana-Champaign, Urbana, Aug. 1999.
- ²¹Press, W. H., Teukolsky, S. A., Vetterling, W. T., and Flannery, B. P., *Numerical Recipes in Fortran—The Art of Scientific Computing*, 2nd ed., Cambridge Univ. Press, New York, 1992, pp. 372–375.
- ²²Gopalarathnam, A., and Selig, M. S., "A Hybrid Approach to Inverse Design of Complex Aerodynamic Systems," AIAA Paper 2000-0784, Jan. 2000.
- ²³Pesonen, U. J., Agarwal, R. K., and Laine, S., "Fast and Robust Viscous/Inviscid Interaction Code for Wing Flowfield Calculations," *Journal of Aircraft*, Vol. 37, No. 4, 2000, pp. 730–733.